Monte Carlo Calculations on Intranuclear Cascades. I. Low-Energy Studies*†

N. METROPOLIS,‡ R. BIVINS, AND M. STORM,§ *Los Alamos Scientific Laboratory, University of California, Los Alamos, New Mexico*
ANTHONY TURKEVICH, *Enrico Fermi Institute for Nuclear Studies, University of Chicago, Chicago, Illinois*
J. M. MILLER, *Columbia University, New York, New York*
AND
G. FRIEDLANDER, *Brookhaven National Laboratory, Upton, New York*
(Received November 26, 1957)

Nuclear cascade calculations of the Goldberger type have been performed using the MANIAC electronic computer. A three-dimensional relativistic treatment was used. The target nuclei were Al^{27}, Cu^{64}, Ru^{100}, Ce^{140}, Bi^{209}, and U^{238}. Incident protons and neutrons with energies between 82 and 365 Mev have been studied, but meson production was neglected in this energy range. Cascades initiated by about 1000 incident particles were followed in each case.

The results have been compared with those of previous calculations of this type, as well as with experimental photographic-plate data and counter measurements reflecting the cascade stage of high-energy nuclear reactions. The agreement with experimental data is usually good.

Tables and graphs are presented showing the frequency of occurrence of various residual nuclei, and data on the residual nuclear excitation energy after the cascade is over. A few comparisons with radiochemical data indicate over-all agreement with the general spallation pattern of copper with 340-Mev protons and good agreement with the $Ni^{64}(p,n)Cu^{64}$ reaction over the energy range 100–400 Mev. However, the calculated results for the $Cu^{65}(p,pn)Cu^{64}$ reaction are low by almost a factor of two, although the energy dependence is approximately correct.

I. INTRODUCTION

THE mechanism of high-energy nuclear reactions of elementary particles with complex nuclei proposed by Serber[1] separates the reaction into two stages. In the first, fast stage, the incoming particle initiates a cascade inside the nucleus. In this stage the interactions are supposed to be with individual nucleons in the nucleus. These interactions are governed by the same cross sections that are applicable in free space but modified by Pauli exclusion effects inside the nucleus. In a second, slow stage, the residual excited nucleus left after the cascade de-excites by the so-called evaporation mechanism.[2]

Calculations implementing the idea of a nuclear cascade have been carried out by Goldberger,[3] Bernardini, Booth, and Lindenbaum,[4] Morrison, Muirhead, and Rosser,[5] McManus, Sharp, and Gellman,[6] Meadows,[7] Combe,[8] Rudstam,[9] and Ivanova and Pianov.[10] They have all been performed by a Monte Carlo technique and the results have been found to agree at least qualitatively with experimental data on nuclear transparencies and the frequency and angular distribution of emitted fast protons. In addition, Meadows,[7] Jackson,[11] and Rudstam[9] have used such calculations as a starting point for evaporation estimates to explain the yields of spallation products observed in radiochemical studies.

In spite of the crudeness of the model it was felt desirable to repeat the previous cascade calculations using a modern electronic computer. The object was to improve the statistics obtained heretofore, to eliminate the approximations made in previous treatments, to utilize the more recent data on elementary cross sections and their angular distributions, and to extend the calculations to higher energies, including, at least crudely, meson production, scattering, and reabsorption effects.

Such calculations would make possible more detailed comparisons of the same type as have been made previously. In addition, having provided a basis for evaluating the validity and limitations of the model, the calculations would furnish a body of data which could be used to make predictions of other quantities. A question of special interest to some of the authors is whether or not a cascade calculation based on the model furnishes a suitable starting point for evaporation

* This work was supported in part by the U. S. Atomic Energy Commission.
† A preliminary report of this work was presented at the January, 1957 New York Meeting of the American Physical Society [Bull. Am. Phys. Soc. Ser. II, 2, 63 (1957)].
‡ Now with the Institute for Computer Research, University of Chicago, Chicago, Illinois.
§ Now with the Midwestern Universities Research Association (MURA), Madison, Wisconsin.
[1] R. Serber, Phys. Rev. **72**, 1114 (1947).
[2] V. F. Weisskopf, Phys. Rev. **52**, 295 (1937).
[3] M. L. Goldberger, Phys. Rev. **74**, 1268 (1948).
[4] Bernardini, Booth, and Lindenbaum, Phys. Rev. **88**, 1017 (1952).
[5] Morrison, Muirhead, and Rosser, Phil. Mag. **44**, 1326 (1953).
[6] McManus, Sharp, and Gellman, Phys. Rev. **93**, 924A (1954); also private communication.
[7] J. W. Meadows, Phys. Rev. **98**, 744 (1955).
[8] J. Combe, Nuovo cimento **3**, S182 (1956).
[9] G. Rudstam, Ph.D. thesis, University of Uppsala, Uppsala, Sweden, 1956 (unpublished).
[10] N. S. Ivanova and I. I. Pianov, J. Exptl. Theoret. Phys. U.S.S.R. **31**, 416 (1956); [translation: Soviet Phys. JETP **4**, 367 (1957)].
[11] J. D. Jackson, Can. J. Phys. **35**, 21 (1957).

TABLE I. Nuclear characteristics of target nuclei (on basis of $r_0=1.3\times10^{-13}$ cm). (All energies in Mev.)

Nucleus	$\pi r_0^2 A^{\frac{2}{3}}$ (b)	Fermi energies p	Fermi energies n	Average binding energy of loosest nucleon[a]	Total nuclear potential p	Total nuclear potential n	Coulomb energy at surface	Cutoff energy[b] T_D
$_{13}Al^{27}$	0.478	27.8	29.5	9.1	36.9	38.6	4.8	42.5
$_{29}Cu^{64}$	0.850	26.7	30.2	8.4	35.1	38.6	8.0	44.9
$_{44}Ru^{100}$	1.144	26.2	30.7	7.9	34.1	38.6	10.5	46.8
$_{58}Ce^{140}$	1.432	25.2	31.7	7.3	32.5	39.0	12.4	48.2
$_{83}Bi^{209}$	1.870	24.4	32.2	6.4	30.8	38.6	15.5	50.2
$_{92}U^{238}$	2.039	24.0	32.7	6.1	30.1	38.8	16.5	50.9

[a] The average binding energy of the loosest nucleon was calculated from the tables and formula of N. Metropolis and G. Reitwiesner, Los Alamos Scientific Laboratory Report NP-1980, 1950 (unpublished).
[b] The cutoff energy (T_D) is taken as the average Fermi energy of neutrons and protons plus the binding energy of the loosest nucleon plus the Coulomb energy for a proton at the surface of the nucleus.

calculations. The results of these could then be compared with radiochemical spallation data at high energies.

This paper covers the calculation of nuclear cascades in various nuclei initiated by nucleons having kinetic energies below 380 Mev. In this energy range, meson production has been neglected. A following paper[12] describes the extension of these calculations to nucleon energies up to 2 Bev, as well as the application of such calculations to pion cascades.

II. NUCLEAR MODEL AND INPUT INFORMATION

The nuclear model used here was the same as that employed in previous calculations, namely, a degenerate Fermi gas of nucleons in a nuclear potential of radius $r_0A^{\frac{1}{3}}$. Almost all the calculations were performed using $r_0=1.3\times10^{-13}$ cm; a few were done with $r_0=1.4\times10^{-13}$ cm for comparison with previous calculations and in order to test the sensitivity of the results to this parameter.

The nuclear characteristics of the target nuclei studied are given in Table I. For each nucleus (column 1), there are given the geometrical cross section on the basis of $\sigma_g=\pi r_0^2A^{\frac{2}{3}}$(column 2), the Fermi energies, $E_F{}^p$ and $E_F{}^n$, of the protons and neutrons (columns 3 and 4), the average binding energy of the loosest nucleon (column 5), and the resultant total nuclear potentials $V_F{}^p$ and $V_F{}^n$ for protons and neutrons (columns 6 and 7). The Coulomb energy at the surface of the nucleus is given in column 8. The particles (both neutrons and protons) were treated as cascade particles until their energies inside the nucleus had fallen below a value T_D. T_D was taken as approximately equal to the kinetic energy a proton would need to overcome the Coulomb barrier at the surface of the nucleus. This cutoff energy is listed in column 9.

The elementary cross sections needed for calculations covered in this paper are the total p-p and n-p scattering cross sections as a function of energy and the differential cross sections as a function of angle in the energy range being considered. The Coulomb contribution to the p-p cross sections was neglected and the n-n cross sections and angular distributions were taken equal to the p-p values. In this energy range only elastic processes were considered. The total cross sections were calculated from the empirical relations:

$$\sigma_{ii}=\left(\frac{10.63}{\beta^2}-\frac{29.92}{\beta}+42.9\right)\text{mb}, \tag{1}$$

$$\sigma_{ij}=\left(\frac{34.10}{\beta^2}-\frac{82.2}{\beta}+82.2\right)\text{mb}, \tag{2}$$

where β is the velocity of the incoming nucleon in units of the velocity of light, σ_{ii} is the cross section when the incoming and struck nucleons are alike, and σ_{ij} is the cross section when they are different.

These cross sections, presented as a function of energy, are given in Figs. 1 and 2. The fit to the experimental points[13–15] in the energy range 25–350 Mev is within 6%.

The angular dependence of the scattering processes in the center-of-mass system was represented by

$$d\sigma/d\Omega=K(A\cos^4\theta+B\cos^3\theta+1), \tag{3}$$

with the constants A and B depending on the type of collision (ii or ij) and on the energy. The constants were put into the computer in the form of a table giving values at eight energies between 0 and 302 Mev

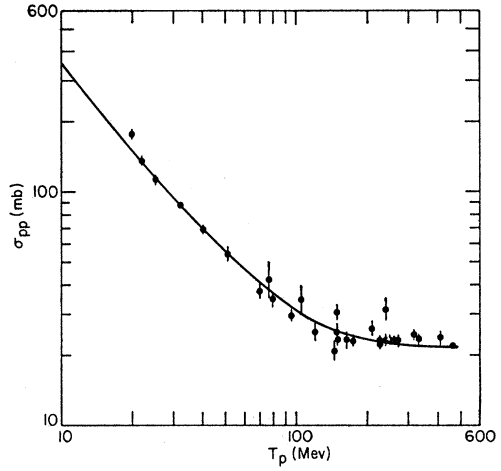

FIG. 1. Total elastic proton-proton scattering cross section, in millibarns, as a function of proton energy, T_p, in Mev. Comparison between analytic expression used in MANIAC calculation (solid curve) and experimental data (points) from references 13, 14, and 15.

[12] Metropolis, Bivins, Storm, Miller, Friedlander, and Turkevich, Phys. Rev. **110**, 204 (1958), following paper.

[13] *Neutron Cross Sections*, Atomic Energy Commission Report AECU-2040 (Technical Information Division, Department of Commerce, Washington, D. C., 1952).
[14] W. N. Hess, University of California Radiation Laboratory Report, UCRL-4639 (unpublished).
[15] Kruse, Teem, and Ramsay, Phys. Rev. **101**, 1079 (1956).

in the center-of-mass system. Linear interpolation was used. The values for these angular-distribution constants are given in Table II.

The functional form of the angular distribution used here does not always quite fit the data[13,14,16] within the experimental errors. In such cases the constants were chosen so that the same fraction of collisions with a stationary nucleon was forbidden as was implied by the experimental data. As is seen from Table II, the n-p scattering is anisotropic even at the lowest energies. The p-p scattering becomes anisotropic only above about 200 Mev (c.m.). The main departure from isotropy is enhancement of scattering forward and backward. In addition, there are slight variations in the ratio of forward to backward scattering in the n-p case (B_{ij}).

The calculation in its present form disregards the possible existence in the nucleus, and interaction with an incoming particle, of aggregates of nucleons. Thus it cannot predict the cascade emission of complex units such as deuterons, tritons, etc.

III. COURSE AND MECHANICS OF THE CALCULATION

The calculation was carried out by a Monte Carlo method as were previous calculations of this type. The Los Alamos MANIAC[17] was used for the computations. The general course of the calculation was also very similar to previous computations of this type and will not be discussed except in the details in which it differs from them. A block diagram of the course of the computation is given in Fig. 3.

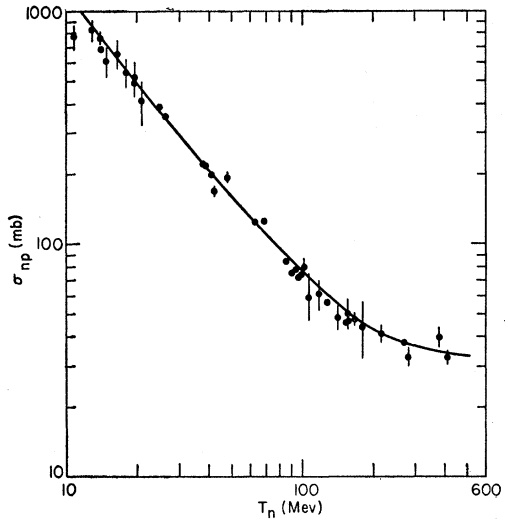

FIG. 2. Total elastic neutron-proton scattering cross section, in millibarns, as a function of neutron energy, T_n, in Mev. Comparison between analytic expression used in MANIAC calculation (solid curve) and experimental data (points) from references 13 and 14.

TABLE II. Constants of the angular distribution of nucleon-nucleon scattering in the center-of-mass system.

$$d\sigma/d\Omega = K(A\cos^4\theta + B\cos^2\theta + 1).$$

T[a] (Mev)	n-n and p-p collisions A_{ii}	B_{ii}	n-p and p-n collisions A_{ij}	B_{ij}
0	0	0	0	0
43	0	0	2.10	−0.22
86	0	0	5.80	−0.70
129	0	0	6.95	−0.56
173	0.05	0	4.30	−0.10
216	0.29	0	3.50	+0.20
259	0.80	0	4.15	+0.50
302	1.85	0	5.35	+0.70

[a] Energy available in the center-of-mass system.

In contrast to most previous calculations, a complete three-dimensional treatment was used throughout. The kinematics of each collision was calculated relativistically. The angles and cosines were selected from appropriate distributions and expressed with greater than five decimal digit accuracy. The mass difference between neutron and proton was neglected, but otherwise the accuracy of the energy calculations was of the order of 0.3 Mev.

The distance of travel of a nucleon was determined from its mean free path. This was calculated from the nuclear composition at the particular stage of the cascade (number of nucleons left in the nucleus), and from the total cross sections, modified appropriately to take into account the slightly increased probability of collisions due to the internal motion of the nucleons of the nucleus when the total cross section has the form of Eqs. (1) and (2). This arises because the probability of collisions with various nucleons in the nucleus depends on the product, $v_r \times \sigma(v_r)$, where v_r is the relative velocity of the incoming particle with respect to a given nucleon, and $\sigma(v_r)$ is the cross section at that relative velocity. As a result of this, the selection of the momentum, η, of the struck nucleon is insignificantly different from a random selection out of an η^2 distribution. However, the direction of motion of the struck nucleon relative to the incident one must be chosen out of a slightly anisotropic distribution, tending to favor overtaking collisions at low energies. A particular distance of travel, d, is obtained from the expression

$$d = -\lambda \ln\xi,$$

where λ is the mean free path and ξ is a uniformly distributed random number in the interval 0 to 1. These random numbers were generated by squaring a 38-bit (binary digit) number and extracting the middle 38 bits of the 76-bit product.[18] The determination of

[16] M. G. Mescheryakov, *Proceedings of the Conference of the Academy of Sciences of the U. S. S. R. on the Peaceful Uses of Atomic Energy, Moscow, July, 1955* (Akademiia Nauk, S. S. S. R. Mowcow, 1955), Plenary Session [English translation: Consultants Bureau, New York: U. S. Atomic Energy Commission Report TR-2435, 1956)].

[17] J. B. Jackson and N. Metropolis, Los Alamos Scientific Laboratory Report, LA-1725, 1951 (unpublished).

[18] L. Cook-Leurgans and N. Metropolis (to be published).

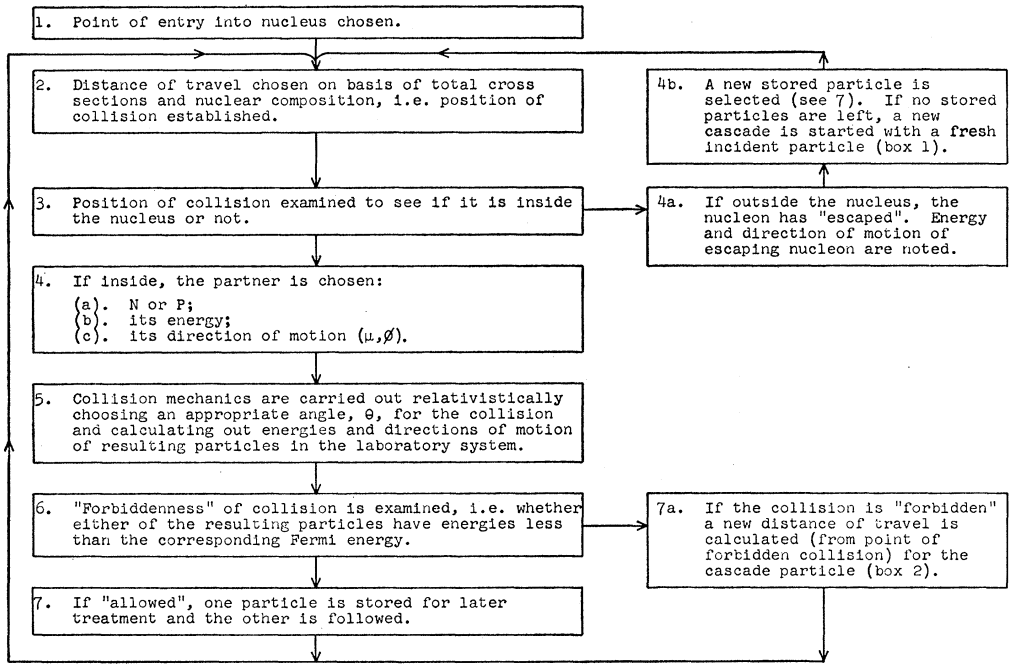

FIG. 3. Block diagram of the course of the Monte Carlo calculation of nuclear cascades performed on the MANIAC.

the distance of travel in this way is typical of the Monte Carlo method used throughout the present work.

To perform the calculation with the required detail, the entire fast memory of the MANIAC (1024 forty-bit words) was utilized. An auxiliary magnetic memory system was used for the storage of data on intermediate cascade particles. Final results from each cascade were recorded permanently on magnetic tape. A typical cascade in this energy region took about five seconds. The standard treatment of one case (a fixed incident energy particle of a particular type on a given nucleus) involved about one-thousand incident particles.

About 35 cases were treated in these low-energy studies. They were chosen to give a moderately good coverage over the complex nuclei of the periodic table and the energy range 75 to 375 Mev. Somewhat fewer cases were run with incident neutrons than with incident protons. The target nuclei studied were Al^{27}, Cu^{64}, Ru^{100} (close to the average of the heavy nuclei in photographic emulsion), Ce^{140}, Bi^{209}, and U^{238}. The incident energies were taken close to 82 Mev, 156 Mev, 236 Mev, 286 Mev, and 365 Mev. The entries in Table V indicate the specific cases studied.

Representations of typical nuclear cascades worked out by the Monte Carlo method have been presented previously[4,8,9] and so are not shown here. The calculation consists of working out the details of many such cascades and then statistically analyzing the results.

As input data for this secondary analysis the computer stored on a magnetic tape, for each incident particle treated, the following information:

1. The type (n or p), energies, and angles of emergence (relative to the incident particle direction and relative to a fixed perpendicular axis) of all escaping particles.
2. The number, type, and energies of the nucleons struck during the cascade.
3. The excitation energy of the residual nucleus.

The above information has, in general, been printed out for only a fraction of the cascades, but has instead been analyzed statistically in various ways by the computer. Some of the results are presented in this paper. Others are available at Chicago, Brookhaven, and Los Alamos.

IV. COMPARISON WITH PREVIOUS CALCULATIONS

In comparing the results of this calculation with previous work of this type, one must bear in mind (a) the increased statistical accuracy of the present calculations, (b) the more rigorous treatment followed here, and (c) the different values of the input parameters (primarily the nuclear radius and cutoff energy) used in the different calculations.

With these considerations in mind we find that the number and energy distribution of the fast cascade particles (e.g., >30 Mev) are given equally well (within statistics) by the different calculations. The angular distributions are hard to compare because of the geometrical approximations assumed in most previous calculations. Finally the average excitation energy and the yield of different cascade products

depend rather sensitively on the nuclear radius used and the cutoff energy. The total inelastic cross section is a less sensitive function of these parameters.

As an example of these generalizations we find that the average number of cascade nucleons is as much as 50% lower than that given by McManus, Sharp, and Gellman[6] who used $1.4\times10^{-13}A^{\frac{1}{3}}$ cm for the nuclear radius, but the excitation energies are 30 to 40% higher. The total inelastic cross sections deduced in this paper (see below) are at most 10% lower than those found by McManus and co-workers. The distribution in excitation energies found by these authors is qualitatively the same as we deduce, except for a smaller tendency in their work to predict "quasi-compound nucleus formation" (see Sec. IX).

Similar remarks apply to the calculation of Meadows[7] who used parameters and approximations of the same type as Bernardini, Booth, and Lindenbaum,[4] and McManus *et al.*[6] In particular, Fig. 4, illustrating the relative frequency of different product nuclei when a medium-weight nucleus ($A\sim64-75$) is bombarded with ~100-Mev and 170-Mev protons, shows the predictions of different calculations. Although the trends are similar, the predicted yields of specific products differ by more than an order of magnitude. In general, the calculations of Rudstam, who used a radius of $1.2\times10^{-13}A^{\frac{1}{3}}$ cm agree somewhat better in detail with the present results than do those performed on the basis of a radius of $1.4\times10^{-13}A^{\frac{1}{3}}$ cm. A striking

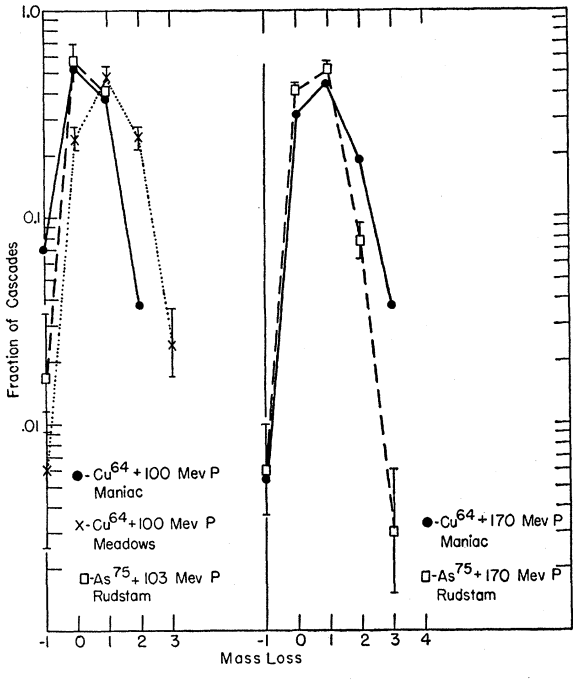

FIG. 4. Relative frequency of prominent cascade products as given by different Monte Carlo calculations. The MANIAC results are interpolated from curves in Fig. 13(a); Meadows' results are from reference 7; Rudstam's results are from reference 9.

TABLE III. Comparison of photographic-plate data with MANIAC results.

(a) ~360-Mev incident protons

Energy No. of prongs	$T>30$ Mev BBL[a]	$T>30$ Mev MANIAC	$T>100$ Mev BBL[a]	$T>100$ Mev MANIAC
0	0.35 ±0.03	0.272±0.019	0.57 ±0.04	0.460±0.024
1	0.54 ±0.04	0.520±0.026	0.40 ±0.04	0.486±0.025
2	0.09 ±0.02	0.194±0.016	0.025±0.010	0.053±0.008
3	0.017±0.007	0.016±0.005		
	100 Mev $>T>$30 Mev			
Average No. of prongs	0.35 ±0.04	0.361±0.022	0.42 ±0.04	0.593±0.028

(b) ~300-Mev incident protons

Energy No. of prongs	90 Mev $>T>$30 Mev Friedman[b]	90 Mev $>T>$30 Mev MANIAC	$T>90$ Mev Friedman[b]	$T>90$ Mev MANIAC
0	0.59 ±0.13	0.67 ±0.03	0.54 ±0.03	0.54 ±0.03
1	0.34 ±0.09	0.28 ±0.02	0.42 ±0.03	0.44 ±0.02
2	0.07 ±0.04	0.05 ±0.01	0.034±0.010	0.023±0.005
3	0.003	0.003	0.005	0
Average No. of prongs	0.49 ±0.13	0.41 ±0.02	0.50 ±0.04	0.48 ±0.03

[a] Data of Bernardini, Booth, and Lindenbaum, reference 20.
[b] Data of J. Friedman, reference 21.

difference, not apparent from Fig. 4, is the relative improbability of cascade neutron emission predicted by Rudstam. Our calculation indicates approximately unity for the ratio of formation of (P,N) to (P,P') and of $(P,2N)$ to $(P,2P)$ cascade products,[19] whereas Rudstam obtains significantly smaller values for these ratios at 103 and 170 Mev.

V. COMPARISON WITH PHOTOGRAPHIC-PLATE DATA

A traditional way of checking the results of cascade calculations has been by comparison with photographic-plate data. Such comparisons are complicated by effects arising in the light nuclei of the emulsion and by varying plate sensitivities and criteria of scanning. The most direct comparison is with the fast (greater than about 30 Mev) protons since these are thought to arise as a direct consequence of the nuclear cascade.

Table III presents a comparison of this type. In the first part, the experimental results of Bernardini, Booth, and Lindenbaum[20] for proton energies between 350 and 400 Mev are compared with a MANIAC run of 364-Mev protons on Ru^{100}. In the second part, a comparison is made between a MANIAC run of 286-Mev protons on Ru^{100} and data obtained by Friedman[21] on G5 emulsion exposed to 310±5 Mev protons from the University of Chicago synchrocyclotron. In this work

[19] In this paper, over-all cascade reactions will be designated by capitals, e.g., (P,PN); over-all nuclear reactions (i.e., including the evaporation stage) by lower case letters, e.g., $Cu^{65}(p,pn)Cu^{64}$. The symbol $\mathfrak{N}$ will be used to denote a nucleon (either a proton or a neutron) participating in a cascade.

[20] Bernardini, Booth, and Lindenbaum, Phys. Rev. **85**, 826 (1952).

[21] J. Friedman, Enrico Fermi Institute for Nuclear Studies, University of Chicago (private communication, May, 1956).

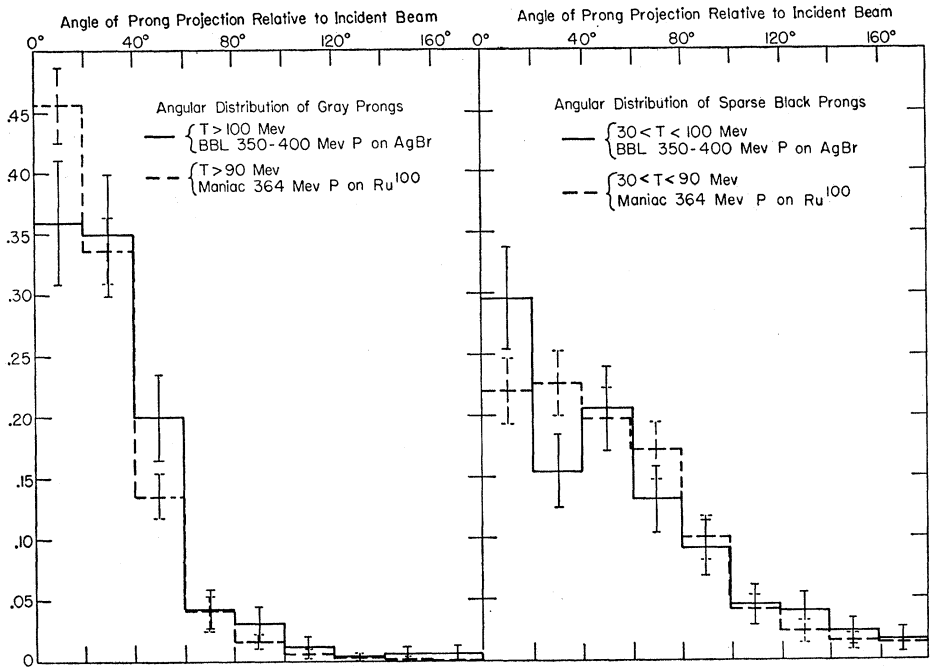

FIG. 5. Angular distribution of fast protons from the ~365-Mev proton bombardment of heavy nuclei. Comparison of the data of Bernardini, Booth, and Lindenbaum[20] with MANIAC calculations. Ordinate: fraction of protons at a given angle; abscissa: angle of prong projection relative to beam direction.

682 stars were found by track scanning and 2800 stars with at least one light prong were found by area scanning.

Table III compares the prong distribution as well as average prong number for protons having energies between 30 and ~95 Mev, and for those with energies greater than ~95 Mev. It is seen that the agreement is moderately good in the case of the comparison with Bernardini *et al.* [Table III(a)] and very good in the case of the comparison with the data of Friedman [Table III(b)].

Figures 5 and 6 present the angular distribution of the fast prongs observed in photographic plates in comparison with that predicted by the MANIAC calculations. It is seen that for both sparse black prongs (~95 Mev$>T\geqslant$30 Mev) and grey prongs ($T>$~95 Mev) the agreement is very good. Figure 5 uses the data of Bernardini, Booth, and Lindenbaum[20] who, however, reported only projected angles; Fig. 6 compares Friedman's data[21] on protons of energy greater than 90 Mev with the results of the calculations.

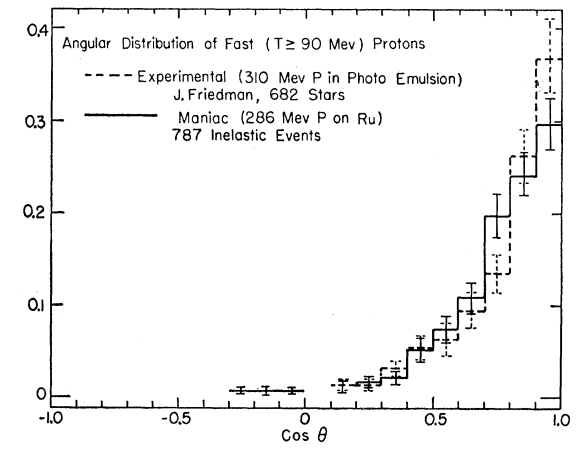

FIG. 6. Angular distribution of very fast (>90 Mev) protons from the ~300-Mev proton bombardment of heavy nuclei. Comparison of the data of Friedman[21] with MANIAC calculations. Ordinate: fraction of protons at a given angle; abscissa: cosine of angle relative to incident beam direction.

A detailed kinetic-energy distribution for the fast protons is not easy to deduce from photographic-plate data. The MANIAC data, however, are in adequate agreement with the sparse data given by Bernardini, Booth, and Lindenbaum.[20] Figure 7 shows a comparison between the fast-proton energy distribution measured by Combe[22] and arising from the interaction of 340-Mev protons with the heavy nuclei of photographic emulsion and the Monte Carlo results from the study of 366-Mev protons on Ru. It is seen that between 100 Mev and 300 Mev the energy distribution calculated agrees well with that observed. The low values found by Combe for the number of protons below 100 Mev are unreasonable; the slight disagreement at the highest energies may well be due, as Combe suggests, to lack of experimental detection efficiency for such particles.

A different type of photographic-plate data is available from the work of Bailey,[23] who measured the energy spectrum of the charged particles produced at various angles in the 190-Mev proton bombardment of Al, Ni, Ag, and Au foils. We have chosen to compare our calculations with the results of Bailey for 30- to

[22] J. Combe, J. phys. radium **16**, 445 (1955).
[23] E. Bailey, University of California Radiation Laboratory Report, UCRL-3334, March 1, 1956 (unpublished).

60-Mev protons emitted at 46° to 65° and 102° to 117° relative to the incident proton beam. The energy range has been selected to test that part of the spectrum due to the cascade; at still higher energies Bailey's experiment may not have detected all protons. The results of the comparison are presented in Table IV. It is seen that in the forward direction (46° to 65°) the agreement is very good for all four target nuclei. In the backward direction (102° to 117°) the MANIAC results tend to be a factor of two lower than the experimental values (except for Au). In view of the large statistical errors and the strong variation in proton yield with energy of the secondary protons in this angular region, the disagreement here is not felt to be serious.

VI. COMPARISON WITH COUNTER DATA

A much more rigid test of these calculations is a comparison with counter measurements of energetic particles produced in the high-energy bombardment of complex nuclei. Here the calculation usually has much poorer statistical accuracy than the measurement. On the other hand the measurements often suffer from poorer resolution than can be established by the calculations. Some typical comparisons are presented.

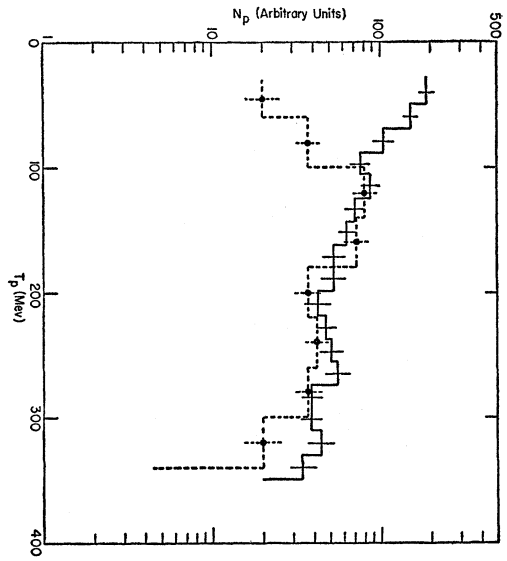

FIG. 7. Kinetic energy distribution of cascade protons from the proton bombardment of heavy nuclei. Dashed line: 340-Mev protons on heavy nuclei in photographic emulsion (Combe[22]) solid line: 366-Mev protons on Ru^{100} (MANIAC calculation).

The energy distribution of the protons emitted at ~15°, 25°, and 45° when copper is bombarded with ~90-Mev neutrons is represented well by the calculations. Figure 8 shows the data of Hadley and York[24] compared with the results of the MANIAC calculations. It is seen that both the absolute values of the cross sections and the variation with energy above 20 Mev at the three angles agree within the statistical errors.

TABLE IV. Comparison of MANIAC results with experimental data of Bailey[a] for 30–60 Mev protons emitted in the 190-Mev proton bombardment of complex nuclei.

Target	$\frac{d\sigma}{d\Omega}$ (mb/sterad) 46°–65° Bailey	MANIAC[b]	$\frac{d\sigma}{d\Omega}$ (mb/sterad) 102°–117° Bailey	MANIAC[b]
Al	18±3	16±2	2.9±0.4	1.5±0.8
Ni	28±4	24±3	5.1±0.9	2.1±0.8
Ag	33±4	36±4	7.8±1.2	3.8±1.3
Au	48±6	43±7	4.9±1.0	6.7±3.8

[a] The results of Bailey are from reference 23.
[b] The MANIAC results quoted here were interpolated between those obtained for energies and target nuclei actually investigated.

Recently experiments on the inelastically scattered protons arising from the interaction of 96-Mev protons with various complex nuclei have been reported by Strauch and Titus.[25] They measured the differential cross section as a function of energy between 40 and

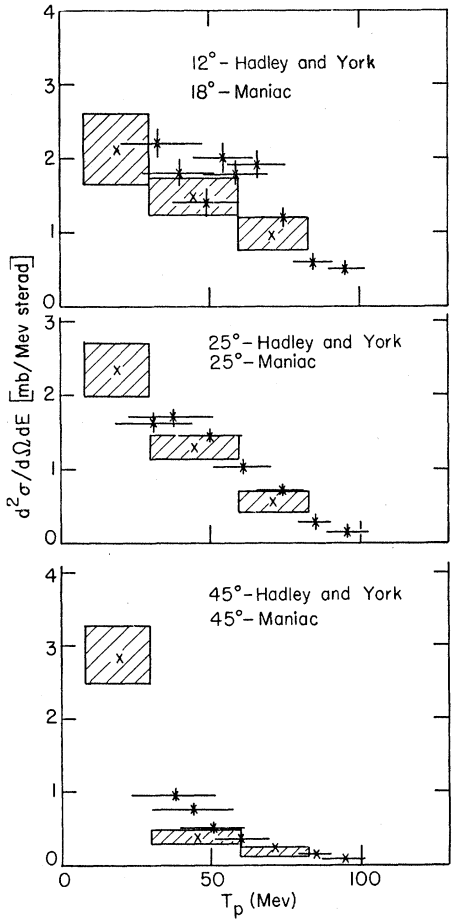

FIG. 8. Kinetic energy distribution of protons emitted at several angles in the interaction of ~90-Mev neutrons with copper. Points: Data of Hadley and York[24] (90-Mev neutrons); shaded rectangles: MANIAC calculations (83-Mev neutrons).

[24] J. Hadley and H. York, Phys. Rev. **80**, 345 (1950).

[25] K. Strauch and F. Titus, Phys. Rev. **104**, 191 (1956).

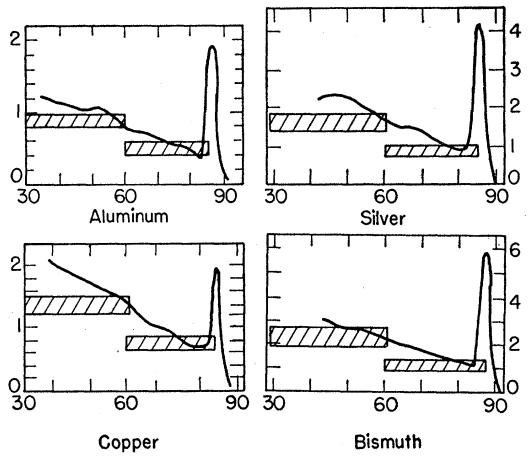

FIG. 9. Comparison of calculated inelastic scattering of 96-Mev protons at ~40° with experimental data of Strauch and Titus.[25] Ordinate: $d^2\sigma/d\Omega dE$ (mb/sterad Mev); abscissa: secondary proton energies (Mev); curve: experimental data of Strauch and Titus; shaded area: MANIAC calculation ($0.7<\cos\theta<0.8$).

90 Mev at an angle of about 40° relative to the incident beam. Their results can be compared rather directly with the results of the MANIAC calculations with incident protons. Since the energy studied in the calculation closest to that of Strauch and Titus was 82 Mev, a slight interpolation was used to convert the results to 96-Mev incident protons. The comparison is made in Fig. 9. In this figure the solid curves are those of Strauch and Titus[25] (the peaks at the highest energy represent the elastically scattered protons). The shaded areas are the results of the MANIAC calculations. Because of the poor statistics these have been combined into two energy regions, 30 to 60 Mev and >60 Mev. The figure indicates moderately good agreement in both absolute values and energy trends. The calculated absolute values tend to be a little lower than the experimental ones.

Less satisfactory is the comparison with the results of Miller, Sewell, and Wright[26] on the angular distribution, between 0° and 70°, of fast neutrons resulting from the bombardment of various elements with 330-Mev protons. These authors used $C^{12}(n,2n)C^{11}$ detectors and found an angular distribution essentially independent of target nucleus between Al and U. Figure 10 shows a comparison of their results (solid curve) with the predictions for the angular distribution of neutrons with kinetic energy greater than 20 Mev from the MANIAC run for 366-Mev protons on Ru (shaded areas). It is seen that the calculation predicts an even broader angular distribution than the experimental results, with probably a maximum at 15° to 30° rather than at 0°. There are two effects which have not been taken into account in the comparison: one, the unknown energy dependence of the $C^{12}(n,2n)C^{11}$ cross section, and two, possible neutron multiplication effects. In spite of this, however, the experimental data at present must be considered at variance with the predictions from the calculation.

[26] Miller, Sewell, and Wright, Phys. Rev. **81**, 374 (1951).

VII. CALCULATED INELASTIC CROSS SECTIONS AND TRANSPARENCIES

It is not to be expected that calculations based on the simple nuclear model used here would reproduce experimental total inelastic cross sections as a function of energy and mass number in complete detail. The value of $r_0=1.3\times10^{-13}$ cm was chosen to give an approximate fit to the observed value of the star production cross section for 305-Mev protons incident on AgBr in emulsions.[21] The resultant MANIAC cross sections for neutrons and protons of various energies on various elements compare as follows with published data.

Figure 11 shows a comparison between the experimentally determined values of inelastic cross sections for high-energy protons and the values predicted by the MANIAC calculation on the basis of $r_0=1.3\times10^{-13}$ cm. The curves give the predicted values as a function of energy for the elements studied. The experimental points are from the measurements and compilation of Millburn, Birnbaum, Crandall, and Schecter[27] with their assignment of ~10% errors. It is seen that there is gross agreement, although the predicted aluminum results tend to be low whereas the ones for Bi seem to be high. Also, if one can trust comparisons between the experimental results of different workers on this subject, the data indicate more of a decrease in cross section with increasing energy than the calculations predict.

The experimental data on total inelastic cross sections for neutrons would appear to be more uncertain than

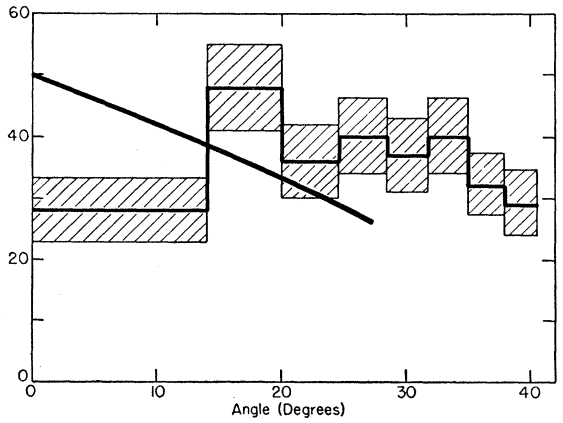

FIG. 10. Angular distribution of fast neutrons from proton bombardments of heavy nuclei. (Ordinates arbitrary.) Histogram: Neutrons with energy greater than 20 Mev as calculated in a MANIAC run of 366-Mev protons+Ru^{100}; curve: $C^{12}(n,2n)C^{11}$ activation from 330-Mev protons on many heavy elements (Miller, Sewell, and Wright[26]).

[27] Millburn, Birnbaum, Crandall, and Schecter, Phys. Rev. **95**, 1268 (1954).

TABLE V. Calculated transparencies for complex nuclei at various bombarding energies.

Target nucleus and geometrical cross section, (mb)	82 Mev	155 Mev	235 Mev	286 Mev	364 Mev
			Incident protons		
Al–478	0.263±0.015		0.275±0.018		
Cu–850	0.176±0.010	0.183±0.009	0.206±0.015	0.202±0.015	0.198±0.015
Ru–1144	0.106±0.009	0.165±0.012	0.154±0.013	0.156±0.013	0.147±0.013
			0.160±0.013[a]		
Ce–1432	0.091±0.009		0.124±0.011		0.114±0.011
Bi–1870	0.064±0.008			0.105±0.008	
U–2039	0.058±0.007	0.074±0.007	0.084±0.009		
			Incident neutrons		
Al–478	0.257±0.015		0.312±0.020		
Cu–850	0.174±0.012	0.238±0.015	0.244±0.016	0.225±0.016	
Ru–1144	0.138±0.011		0.188±0.015		
Ce–1432					
Bi–1870					
U–2039	0.096±0.009		0.146±0.012		

[a] Double entries indicate separate runs of ~1000 incident particles each.

those for protons. Using the compilation and analysis of Millburn, Birnbaum, Crandall, and Schecter,[27] we find that the predictions of the present calculations are 10 to 30% lower than the experimental data at around 90 Mev. In the region of 270 to 300 Mev, the predictions for copper and lead are within the spread of the experimental results. The one experimental value for aluminum in this energy region is 20% higher than that predicted.

The transparency of a nucleus is defined as the difference from unity of the ratio of the experimental inelastic cross section to the geometrical cross section. This latter depends, of course, on the nuclear radius assumed. The existence of an appreciable transparency was historically one of the first indications of the applicability of the present model of high-energy nuclear reactions. In the present calculation, the transparency of a nucleus is determined by the fraction of incident particles that go through a nucleus without interacting. The values that we calculate, using our standard radius parameter of $r_0=1.3\times10^{-13}$ cm, are presented in Table V. A radius parameter of 1.4×10^{-13} cm gives transparency values for Ru^{100} 0.03 to 0.05 higher than those with the smaller radius parameter.

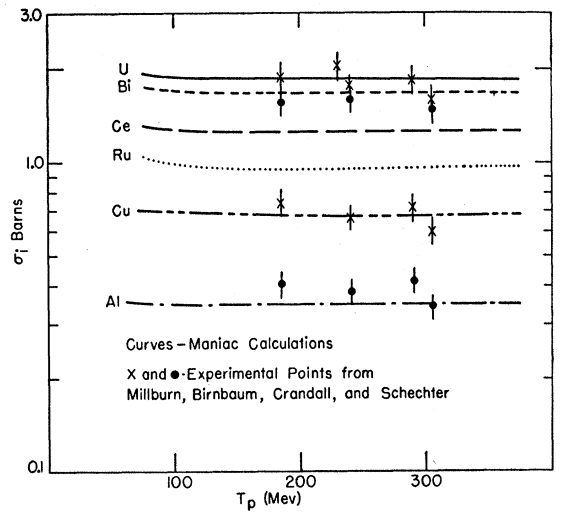

FIG. 11. Comparison of calculated inelastic proton-nucleus cross sections with experimental values. (Experimental points taken from compilation of Millburn, Birnbaum, Crandall, and Schecter.[27])

The results indicate transparencies varying from about 27% for aluminum down to 5 to 10% for uranium. The transparencies tend to be higher for incident neutrons than for protons, especially for the heavier nuclei. This is reasonable because in this energy range the *n-p* cross section is 1.5 to 2.5 times higher than the *p-p* or *n-n* cross section and of course the *n/p* ratio increases in the heavier nuclei.

The transparencies are rather insensitive to the incident energy in the region from 155 to 364 Mev. This presumably arises from two compensating effects: the importance of the Pauli principle in excluding collisions is less at higher energies and this tends to decrease the mean free path of the incoming nucleon. On the other hand, the total elementary cross sections decrease with increasing energy, this effect tending to increase the mean free path. If the average effective nucleon-nucleon cross section, inside the nucleus, σ_{eff}, is given by the Goldberger formula[3]:

$$\sigma_{\text{eff}}=\sigma_t\left(1-\frac{7}{5}\frac{E_F}{E_i}\right),$$

where E_F=Fermi energy, and E_i=incident particle energy inside the nucleus, and σ_t=free nucleon-nucleon cross section, then $(\sigma_{n-p})_{\text{eff}}$ drops only from 38 to 31 mb in going from 82-Mev incident protons to 286-Mev protons. $(\sigma_{p-p})_{\text{eff}}$ is constant at 19±1 mb. This conclusion would be only slightly modified for a larger nuclear radius. If we had chosen 1.40×10^{-13} cm for r_0, the variation in σ_{eff} would be only slightly greater [42.5 to 32 mb for $(\sigma_{n-p})_{\text{eff}}$ in the energy range 82 to 286 Mev].

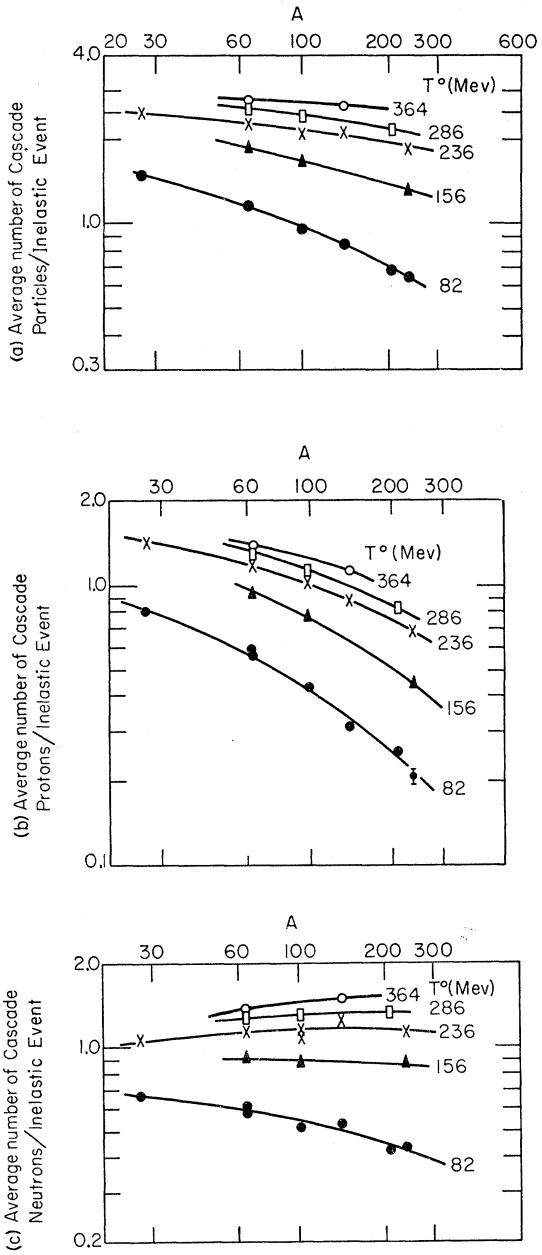

FIG. 12. Calculated average number of (a) cascade nucleons, (b) cascade protons, and (c) cascade neutrons per nuclear interaction as a function of the target nucleus in proton bombardments at various bombarding energies.

It appears from the MANIAC calculations that this predicted insensitivity of the transparency to incident energy is not seriously affected by the asymmetry of the *n-p* scattering.

VIII. NUMBERS AND TYPES OF CASCADE PARTICLES: THE NATURE OF THE RESIDUAL NUCLEI

The variation in the average number of escaping cascade particles, in the number of escaping cascade protons, and in the number of escaping cascade neutrons as a function of target nucleus and energy of the bombarding protons, is presented in Figs. 12(a), 12(b), and 12(c). The average number of escaping cascade particles varies from about 0.65 for uranium at 82 Mev to almost 3 (indicated for aluminum at the highest energy—364 Mev). The general variation is not surprising—a decrease with increasing atomic weight and an increase with increasing energy. The increase with energy is slightly less than linear for uranium and closer to a square root dependence for copper. The total number of escaping cascade particles is very closely the same when neutrons are used as bombarding particles.

The neutron to proton ratios of the outgoing cascade particles are presented in Table VI. There is a striking increase in this ratio as the mass of the nucleus is increased, particularly at low energies. For example, 82-Mev protons on aluminum give rise to a ratio of 0.8 whereas the same energy protons on uranium give a corresponding ratio of greater than 2. A similar rise is observed for incident neutrons. The same effect was observed by McManus, Sharp, and Gellman[6] who calculated an N/P ratio of 2.6 and 4.3 for incident protons and neutrons, respectively, on uranium at 90 Mev.

The large cascade neutron emission from heavy nuclei is considered to arise from two sources: In the first place the *n-p* scattering cross section in this energy region is much higher than the *p-p* and *n-n* cross sections. This means that neutron mean free paths in heavy nuclei (with their neutron excess) will be larger than proton mean free paths. In the second place the following details of our model also enhance neutron emission: The cutoff energy (the energy below which particles are not followed) has been chosen the same for both neutrons and protons. Because of the different numbers of the two types of particles, the neutron Fermi energy is a larger fraction of this cutoff energy than is the proton Fermi energy. Thus neutrons of just above the cutoff will have enhanced mean free paths as compared with protons of the same energy, and so will escape more frequently. It is interesting that these

TABLE VI. Calculated neutron/proton ratio of emerging cascade particles.

Bombarding energy (Mev)	Al	Cu	Ru	Ce	Bi	U
		Incident protons				
82	0.82	1.06, 1.00[a]	1.19	1.17	1.67	2.10
156		0.94	1.14			
236	0.74	0.96	1.06, 1.13[a]	1.41		1.62
286		0.98	1.12		1.60	
364		0.99		1.32		
		Incident neutrons				
82	1.82	2.43	2.80			4.15
156		1.93				
236	1.72	2.11	2.23			3.28
286		2.04				

[a] Double entries indicate separate runs of ~1000 incident particles each.

mechanisms provide additional reasons (besides the intrinsic neutron excess and the Coulomb barrier) for high neutron emission from heavy elements.

The distribution in numbers of cascade particles represents the relative frequency of different changes in mass number of the target nucleus as a result of the cascade part of the high-energy nuclear interaction. In Fig. 13 are presented data on copper, ruthenium, and uranium indicating the fraction of the inelastic events giving rise to a given mass number at the end of the cascade as a function of incident proton energy. The

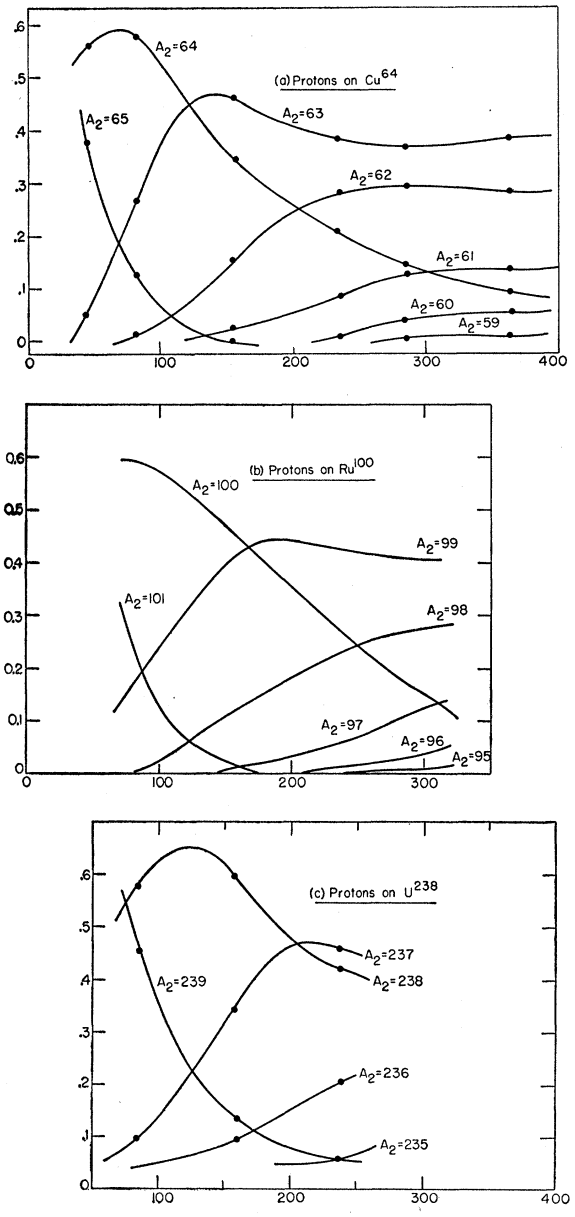

FIG. 13. Calculated yields of a given mass number, A_2, as a result of proton-initiated nuclear cascades. (a) Cu^{64}; (b) Ru^{100}; (c) U^{238}. Ordinate: fraction of total inelastic cross section; abscissa: proton bombarding energy in Mev.

TABLE VII. Calculated average excitation energies (Mev).

Bombarding energy (Mev)	Al	Cu	Ru	Ce	Bi	U
		Incident protons				
82	36.9	46.9, 45.9[a]	53.9	58.3	62.3	63.6
156		54.5, 57.9[a]	66.5			87.0
236	42.2	60.8	72.5, 70.8[a]	85.3		101.1
286		64.5	76.0		104.1	
364		64.5		99.6		
		Incident neutrons				
82	36.2	45.1	50.2			59.0
156		51.8				
236	42.2	57.8	71.6			98.8
286		61.3				

[a] Double entries indicate separate runs of ~1000 incident particles each.

curves for $\Delta A=1$ for the different target elements give the fraction of the cascades leading to compound nucleus formation. For all targets, this fraction decreases with increasing energy and increases with atomic weight. For 100-Mev incident protons, such compound nucleus formation represents some 30% of all inelastic interactions with uranium, but only 6% of all inelastic interactions with copper.

One-particle cascades ($\Delta A=0$) are the dominant mode of interaction in the energy region around 90 Mev; their abundance falls off gradually but continually up to the highest energies studied here.

Aside from this decreasing incidence of zero-particle and one-particle cascades as the energy is raised, the main impression from the graphs of Fig. 13 is that the relative abundance of each of the other important types of cascades (two, three, or four particles out) tends toward a constant value as the energy approaches meson production thresholds. This is best illustrated by the graph for copper, for which cascades were run with 364-Mev incident protons.

IX. EXCITATION ENERGY OF RESIDUAL NUCLEI

The energy of excitation of a residual nucleus at the end of a cascade, E^*, is the sum of the excitations due to "holes" in the degenerate nucleon gas and due to excited nucleons. This is equivalent to calculating it via the formula

$$E^*=T_0^0-\sum_{i=0}^{m} T_i^0-(m-1)B,$$

where T_0^0 is the energy of the incoming particle (in the lab system), T_i^0 is the energy of an outgoing cascade particle (in the lab system), m is the number of outgoing particles, and B is the average binding energy of the m outgoing nucleons.

The excitation energy will in general depend upon the type of cascade. For example, for a cascade with no emerging particles the excitation energy must be a maximum and equal to the incident particle energy plus its binding energy. The average excitation energy

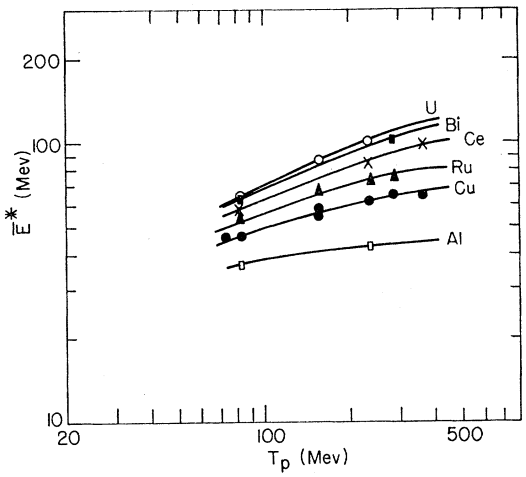

FIG. 14. Calculated average excitation energy ($\bar{E}^*$) in various target nuclei as a function of proton bombarding energy, T_p.

over all inelastic events as a function of incident energy and target nucleus for incoming protons and neutrons is given in Table VII. The data for bombarding protons are presented graphically in Fig. 14. The table and figure show that incoming particles with greater than 100-Mev kinetic energy leave on the average only a fraction of their kinetic energy as excitation energy in the residual nucleus. This fraction is a little more than three-quarters for heavy nuclei at low energies (e.g., uranium at 82 Mev) but is barely more than one-tenth for the light nuclei at the highest energies (e.g., extrapolated value for Al at 364 Mev). Qualitatively this is in agreement with the original predictions of Serber[1] and the results of previous cascade calculations.[3–10] As pointed out by McManus, Sharp, and Gellman,[6] the average excitation energy increases only slowly with bombarding energy—increasing less than a factor of two for an increase of a factor of five in bombarding energy. As is to be expected, energy deposition is greater in the larger nuclei. Energy deposition by neutrons is very close to that by protons.

The absolute values of the excitation energies in this

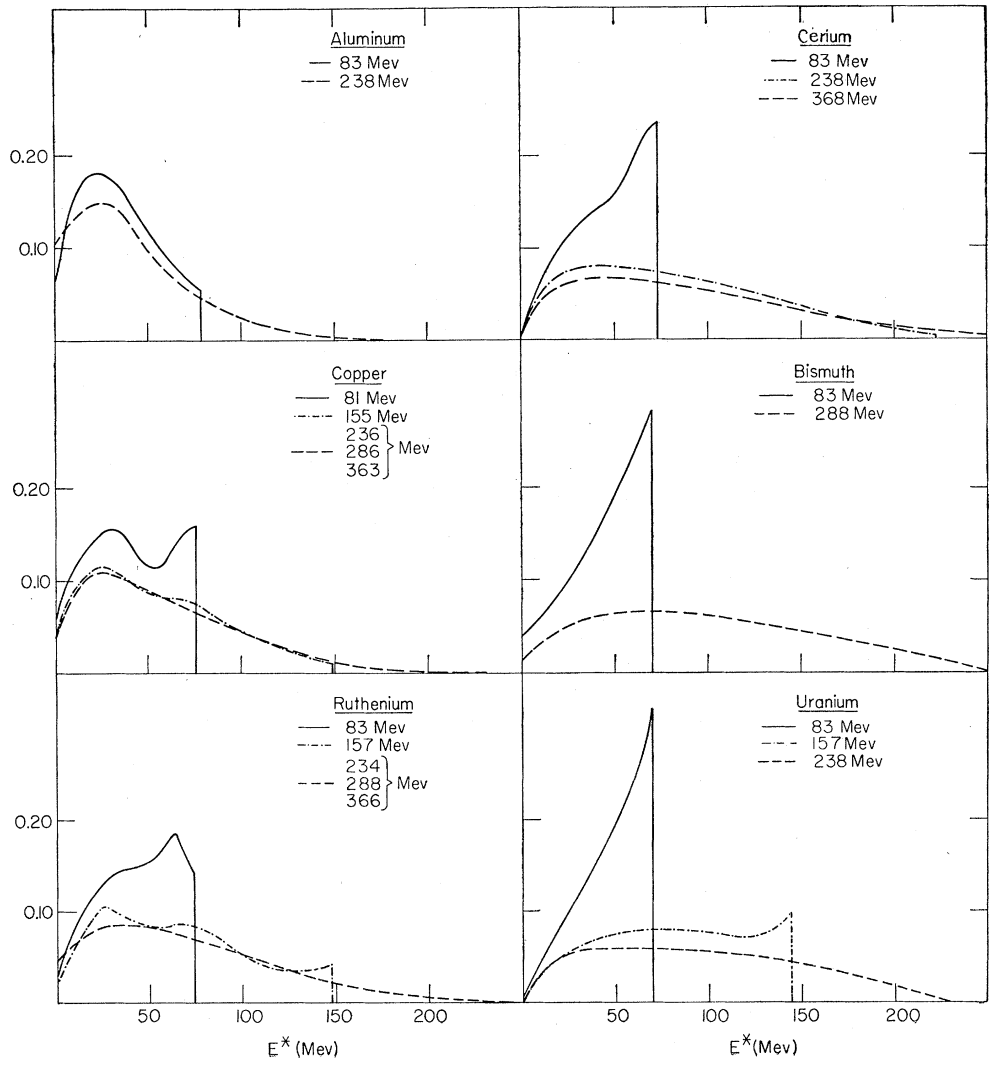

FIG. 15. Calculated gross distribution of excitation energies, $N(E^*)$, for various elements at different proton bombarding energies. (Compound nucleus cases not included.) Ordinate: $N(E^*)$ in units of (10 Mev)$^{-1}$; abscissa: excitation energies, E^*, in Mev.

TABLE VIII. Comparison of calculated excitation energies for 190-Mev incident protons with experimental values.[a]

Element	Gross	MANIAC[b]
Al	50±8	42
Ni	57±9	···
Cu	···	59
Ru	···	69
Ag	69±12	···
Au	83±17	···
Bi	···	90
U	88±17	94

[a] The experimental data are those of Gross, reference 28.
[b] The MANIAC values are interpolated from data in Fig. 14.

study are somewhat higher than predicted by most previous Monte Carlo calculations. This is in part a result of the smaller radii used here as compared to the ones used by most earlier workers. In addition our cascades have been stopped at somewhat higher cutoff energies than were the cascades in previous calculations.

The results we calculate are in excellent agreement with the recent experimental values of Gross,[28] who used measurements of low-energy neutron production to deduce average excitation energies of residual nuclei resulting from the 190-Mev proton bombardment of various targets. The comparison is presented in Table VIII. Even in the case of aluminum, where the agreement is least satisfactory, the MANIAC result is within the experimental error of Gross' number. The experimental values are much higher than those calculated by McManus, Sharp, and Gellman.[6]

In the cascades leading to compound nucleus formation, the excitation energy is unique and is equal to the bombarding kinetic energy plus the binding energy of the particle. In the cascades not leading to compound nucleus formation, there is, of course, a distribution in excitation energies determined by the energies and numbers of outgoing cascade particles. The distribution in excitation energies at various bombarding proton energies for these non-compound-nucleus-forming cascades is presented in Fig. 15. The figure gives the fraction of the time that the residual excitation lies in a 10-Mev energy interval as a function of the position

TABLE IX. Calculated average excitation energies $\bar{E}^*$ (with root-mean-square deviations) for various mass changes resulting from cascades. (Incident protons.) (All energies in Mev.)

Bombarding energy	Al	Cu	Ru	Ce	Bi	U
			$\Delta A=0$			
82	40.8±22.0	45.7±20.9	48.1±18.9	49.8±18.0	48.3±17.9	48.7±16.7
155		59.7±38.9	73.4±43.6			87.8
235	34.7±27.2	52.6±39.4	64.3±54.8	81.3±62.7		102.5±66.0
286		49.2±35.0	67.8±45.7		105.7±72.1	
364		45.2±28.2	54.2±47.2	66.3±54.5		
			$\Delta A=1$			
82	29.7±17.5	28.8±16.1	28.7±14.7	29.4±13.5	26.5±13.3	27.0±13.2
155		52.1±33.8	60.2±33.8			68.5
235	33.5±29.3	53.7±45.3	65.4±46.6	84.6±51.2		97.6±53.0
286		53.5±48.5	68.1±51.8		100.6±62.7	
364		48.0±46.1	65.6±55.7	86.2±69.7		
			$\Delta A=2$			
82	23.8± 9.9	26.1± 7.8	15.0± 4.1			
155		51.6±25.0	54.0±22.6			51.0
235	49.4±33.3	73.5±41.5	81.4±42.8	89.8±42.7		95.8±39.6
286		73.6±47.2	88.4±48.5		113.1±52.1	
364		67.7±38.8	93.6±58.4	118.1±69.3		
			$\Delta A=3$			
155		50.2±17.4	54.6±19.5			
235	59.9±25.6	75.7±34.0	86.1±37.5	93.6±36.0		85.9±32.6
286		87.8±44.1	90.3±37.9		118.4±39.5	
364		95.7±47.8	110.5±55.0	125.5±56.1		
			$\Delta A=4$			
235	75.9±29.0	63.3±24.1	54.9±16.6	79.0±28.7		
286		92.0±37.7	85.9±31.9		94.6±50.9	
364		112.7±50.4	130.5±50.9	118.9±59.3		
			$\Delta A=5$			
235	63.9±35.1					
286		103.0±24.7	90.0± 9.8			
364		111.2±28.3	121.6±52.1	118.7±27.4		

[28] E. E. Gross, Bull. Am. Phys. Soc. Ser. II, 2, 14 (1956); see also University of California Radiation Laboratory Report, UCRL-3330, February 29, 1956 (unpublished) and University of California Radiation Laboratory Report UCRL-3337, March 8, 1956 (unpublished).

TABLE X. Calculated average excitation energies $\bar{E}^*$ (and their root-mean-square deviations) following specific type cascades. (Incident protons.) (All energies in Mev.)

Bombarding energy	Al	Cu	Ru	Ce	Bi	U
			(*P*,*N*) cascades			
82	41.6±21.2	49.1±20.5	51.3±19.0	53.0±18.0	52.6±17.5	52.5±15.9
155		66.4±42.0	76.8±46.8			94.8
235	34.8±27.7	55.8±43.6	65.8±59.2	83.5±65.1		114.0±68.1
286		44.9±34.6	72.9±47.4		115.5±77.3	
364		43.7±28.4	52.3±53.1	75.6±47.5		
			(*P*,*P'*) cascades			
82	40.4±22.4	42.3±20.7	44.3±18.1	44.6±16.7	41.1±16.2	40.7±15.4
155		54.4±35.3	70.0±39.8			76.8
235	34.6±26.8	50.2±35.6	63.0±50.8	78.6±59.4		86.8±59.4
286		52.4±34.9	63.5±43.9		94.4±63.8	
364		46.0±28.0	55.4±43.3	59.4±58.2		
			(*P*,2*N*) cascades			
82	38.2±14.5	37.7±15.6	36.8±14.2	36.5±10.5	33.9±13.2	34.7±10.5
155		63.6±33.3	73.7±32.7			81.2
235	50.4±35.0	84.7±47.3	86.3±44.0	106.1±46.0		116.5±47.8
286		83.2±54.6	93.2±52.2		124.0±58.8	
364		87.3±58.8	88.3±57.7	103.6±67.5		
			(*P*,*PN*) cascades			
82	28.9±17.5	27.3±16.0	26.7±13.8	26.1±13.1	24.3±11.2	22.5±12.3
155		51.5±34.1	57.3±33.1			58.4
235	32.4±27.0	46.6±41.8	61.6±45.3	78.3±53.7		90.4±52.4
286		50.6±47.6	67.8±53.6		93.6±60.5	
364		40.8±39.0	60.9±53.9	79.2±66.9		
			(*P*,2*P*) cascades			
82	26.3±17.2	24.5±13.5	23.5±13.6	17.8±12.6	10.0± 7.3	
155		44.5±30.9	49.5±31.2			42.3
235	29.3±28.9	46.2±41.0	50.8±44.6	66.6±40.0		77.0±53.1
286		43.5±39.9	50.4±37.7		72.9±61.5	
364		39.0±37.7	57.9±53.2	83.3±75.3		
			(*P*,3*N*) cascades			
82						
155		58.8±26.4	65.5±21.4			61.1
235	66.0±32.4	93.8±36.7	97.5±37.3	113.1±37.6		115.6±35.7
286		81.1±48.5	103.0±42.4		138.5±47.1	
364		81.3±21.4	125.5±73.6	164.0±71.3		
			(*P*,*P*2*N*) cascades			
82	24.4±10.6					
155		52.7±23.8	54.1±22.9			52.3
235	52.4±33.5	82.5±43.1	89.3±42.7	89.1±42.3		88.4±39.0
286		80.2±47.9	88.3±51.1		108.7±50.1	
364		68.2±40.6	87.4±51.8	115.7±63.8		
			(*P*,2*PN*) cascades			
82	22.8± 9.6					
155		49.3±25.9	48.4±21.2			30.0
235	46.5±33.0	64.3±38.5	65.0±40.6	77.5±41.0		97.1±36.7
286		65.8±44.1	84.6±47.4		99.1±53.9	
364		65.4±39.9	94.9±58.4	102.3±65.2		
			(*P*,3*P*) cascades			
82						
155		47.9±23.1	59.4±19.7			
235	47.8±32.2	56.3±32.3	69.6±36.3	69.8±33.6		
286		77.0±51.3	74.8±37.1			
364		60.9±38.4	65.3±33.5	84.9±62.8		
			(*P*,4*N*) cascades			
155						
235				120.7±23.4		
286			96.4±41.5		132.8±49.0	
364		104.5±32.2	142.1±61.1	166.5±57.0		
			(*P*,*P*3*N*) cascades			
155		53.2±20.9				
235	59.9±24.8	80.9±34.3	100.8±42.5	93.6±36.5		75.3±27.8
286		86.2±43.3	94.3±42.6		117.1±37.8	
364		102.7±53.2	127.7±53.4	140.1±48.8		

TABLE X.—*Continued.*

Bombarding energy	Al	Cu	Ru	Ce	Bi	U
			(P,2P2N) cascades			
155		44.5±10.2	52.8±17.2			
235	65.1±25.5	73.9±33.2	72.8±30.7	85.3±38.2		
286		91.4±48.5	92.9±28.8		114.4±36.9	
364		95.5±50.8	92.8±47.4	110.0±53.8		
			(P,3PN) cascades			
155		53.8±19.0				
235	54.1±24.6	75.6±37.7	78.2±26.3	93.3±29.5		
286		81.0±32.1	64.0±41.7			
364		86.6±38.6	97.4±55.6	85.9±39.6		
			(P,4P) cascades			
155						
235						
286						
364			107.9±50.1			

of the interval in Mev for each target element. Note that the maximum excitation energy possible is 5 to 17 Mev less than the bombarding energy because of the cutoff energy for outgoing cascade particles.

Figure 15 indicates that the spread of excitation energies about the average is always very wide. At high energies of the bombarding particle there is a tendency for the distribution in the residual excitation energy to resemble a Maxwellian curve with a peak at an energy that is rather independent of the incident energy for a given target nucleus. This is illustrated by the two curves for aluminum and by the curves for copper, ruthenium, and cerium with incident protons having energies greater than 100 Mev. The curves for

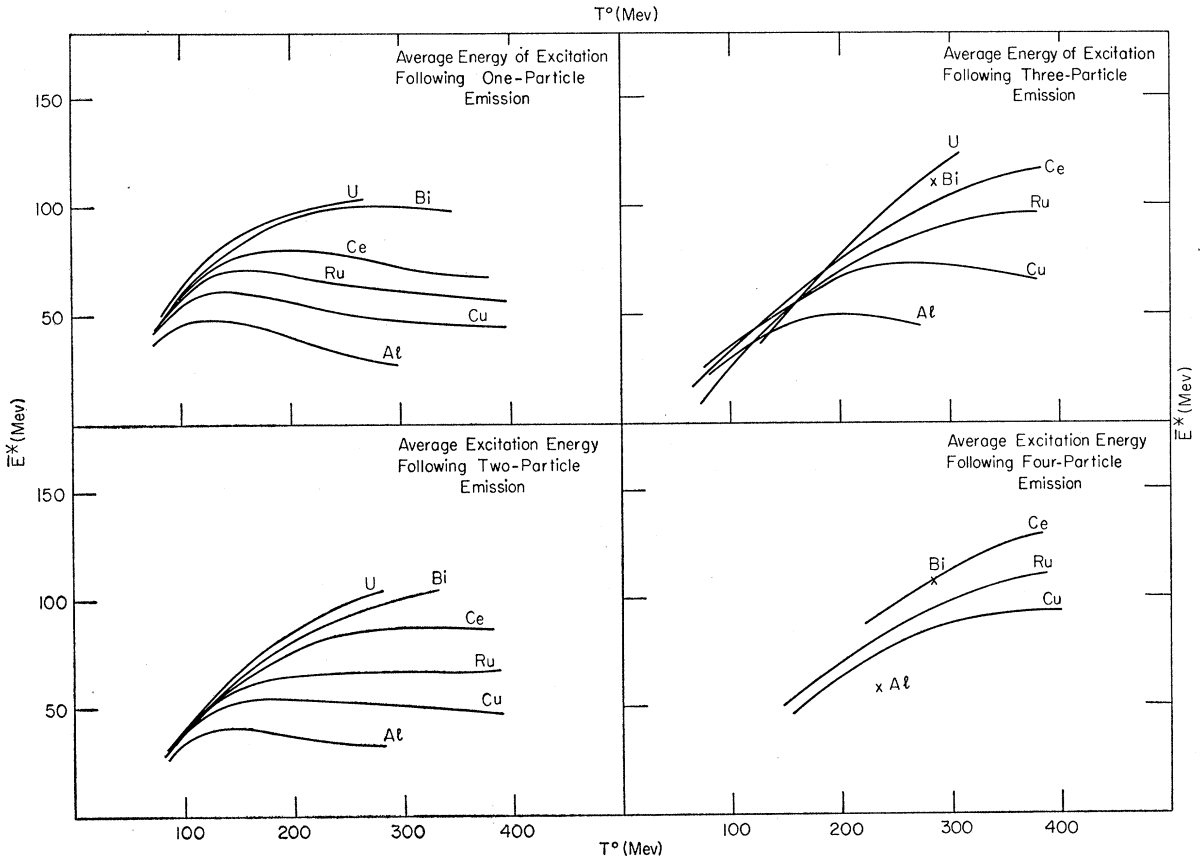

FIG. 16. Calculated average excitation energy, $\bar{E}^*$, associated with specific mass changes in proton-initiated cascades in various nuclei as a function of bombarding energy, T^0.

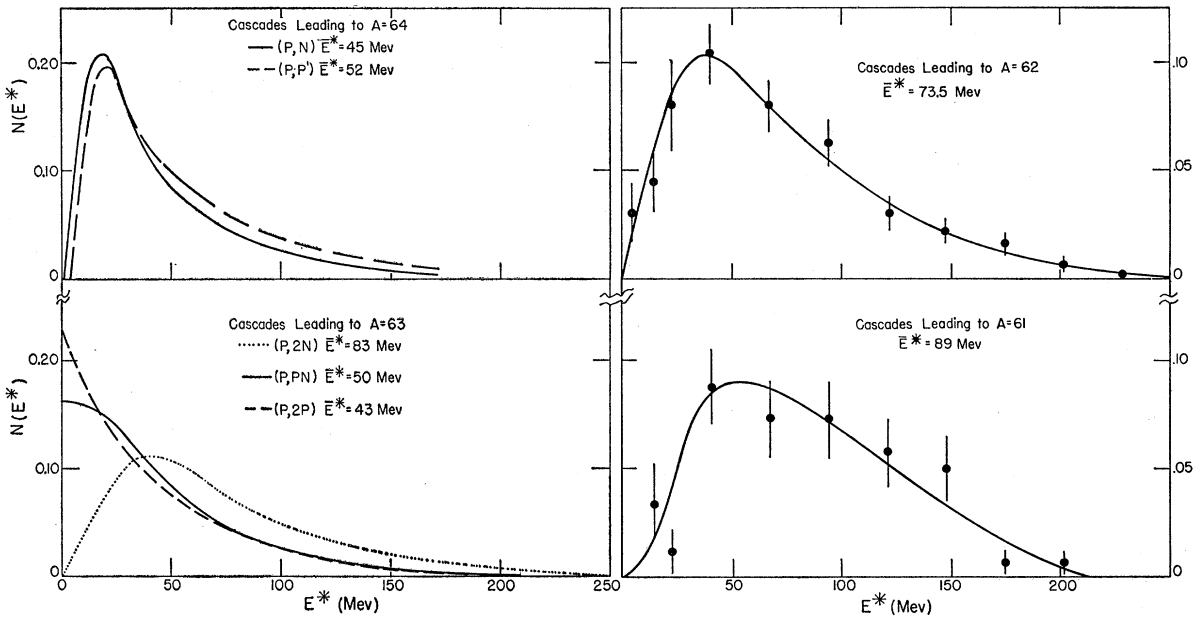

FIG. 17. Calculated distribution of excitation energies, $N(E^*)$, associated with particular type cascades in Cu^{64} initiated by 286-Mev protons. $N(E^*)$ is given in units of $(10\ \text{Mev})^{-1}$. The statistical (standard deviation) errors from the calculation are indicated in the cases where they are appreciable.

a given target differ mainly in the high-energy components of the distributions.

For low-energy nucleons incident on heavy nuclei there is a pronounced peak in the excitation energy distributions at or near the maximum energy possible. This phenomenon may be qualitatively designated as "quasi-compound nucleus" formation.

The average excitation energy associated with a given mass change due to the cascade is presented in Table IX for various proton bombarding energies and for various target nuclei. Values are indicated in the tables only for those cases where at least five cascades contributed. Also given are the root-mean-square deviations from the averages. The average values are presented graphically in Fig. 16. It is seen from the figures that at low-bombarding energy (82 Mev) the average excitation energy is rather independent of the target nucleus, but at the higher bombarding energies the average excitation energy for a given mass change increases markedly with the mass number of the target nucleus.

The calculated average excitation energies for particular types of cascades, (P,N), (P,P'), (P,PN),[19] etc., are presented in Table X together with the root-mean-square deviations of the excitation energy distributions. Only those cases are listed where there were five or more cascades contributing.

As examples of the distributions in excitation energy following particular types of cascades, there are presented in Fig. 17 the distributions following (P,N), (P,P'), $(P,2N)$, (P,PN), $(P,2P)$, $(P,3\mathfrak{N})$, and $(P,4\mathfrak{N})$ cascades in the interaction of 286-Mev protons with copper (all the "three nucleon out" and all the "four nucleon out" cascades have been combined to increase the statistical accuracy).

From Fig. 17 it is clear that many of the distributions in excitation energy have a Maxwellian shape, starting at zero, going through a maximum and then dropping off exponentially. This is definitely not true for the (P,PN) and $(P,2P)$ cascades (see Fig. 17). The distributions in these cases for all incident energies and target nuclei appear to have an appreciable—often a maximum—probability near zero excitation energy. There appears to be no such behavior among the "one nucleon out," "three nucleon out," or "four nucleon out" cascades.

This distinctive feature of the excitation energy distributions connected with the (P,PN) and $(P,2P)$ cascades appears to be related to the possibility in these cases of important contributions from cascades involving only one nucleon-nucleon collision in the nucleus (the struck nucleon being close to the top of the Fermi distribution) with both resultant particles emerging without further interactions.

Finally, in Figs. 18 and 19 we present the change in the distribution of excitation energy following cascades, with one escaping nucleon, at a given incident nucleon energy as the target is varied from aluminum to uranium. Figure 18 is for ~82-Mev incident protons; Fig. 19 for 236-Mev protons. At the lower energy and the largest nucleus the distribution is peaked near the maximum in the already mentioned quasi-compound-nucleus manner; at the higher energy and lightest

nuclei, the distribution is Maxwellian in shape. The other cases appear to be intermediate in character.

X. SOME COMPARISONS WITH RADIOCHEMICAL DATA

One of the main purposes of performing these calculations was to get information which could be used to interpret radiochemical data on spallation cross sections. In general, the comparison with experimental data

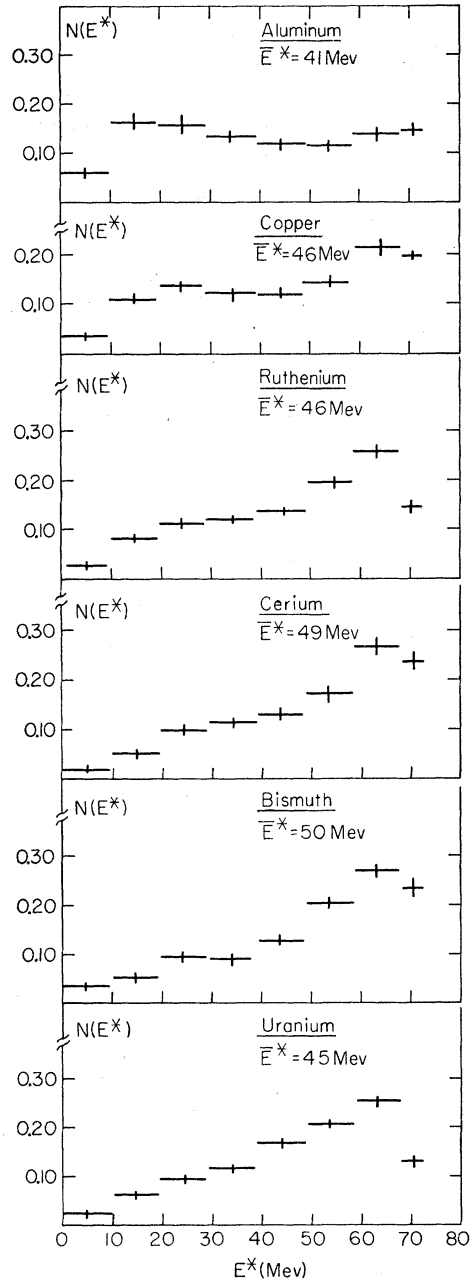

FIG. 18. Distribution of excitation energies, $N(E^*)$, associated with cascades having only one emerging nucleon. (82-Mev incident protons.) $N(E^*)$ is given in units of (10 Mev)$^{-1}$.

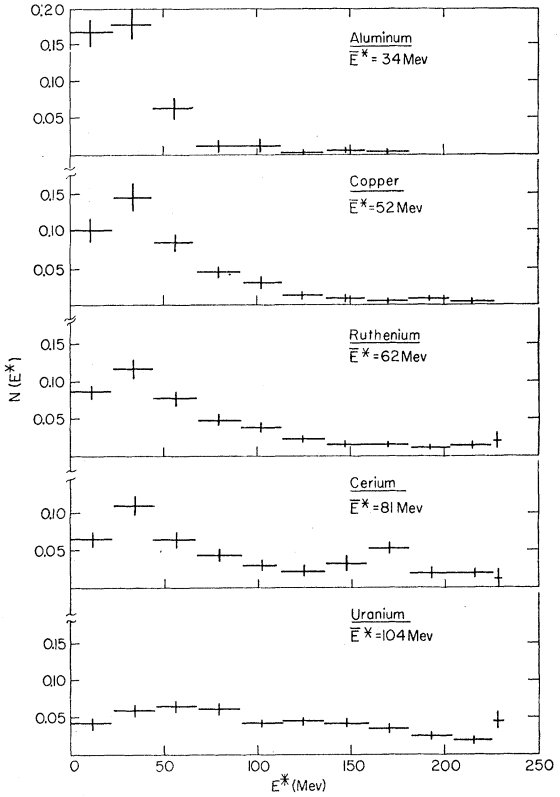

FIG. 19. Distribution of excitation energies, $N(E^*)$, associated with cascades having only one emerging nucleon. (286-Mev incident protons.) $N(E^*)$ is given in units of (10 Mev)$^{-1}$.

requires the use of an evaporation calculation starting with the excited nuclei resulting from the nuclear cascade. At present no such calculations comparable in detail to the cascade calculations have been performed. However, some comparisons with radiochemical data are possible without detailed knowledge of the evaporation phase of the reactions.

One of the simplest reactions which may be considered is the (p,n) reaction.[19] For energies at which meson production is not important, a (p,n) reaction must result directly from a cascade in which a neutron alone is ejected, and the residual excitation is less than that needed to evaporate a nucleon. Figure 20 shows a comparison of calculated and experimental results for the $Ni^{64}(p,n)Cu^{64}$ reaction. The ordinate is the cross section in mb; the abscissa, the incident proton energy. The experimental results are those of Koch and Turkevich.[29] The statistical errors are large in the calculated values because of the low probability of this reaction. The agreement is seen to be excellent in both absolute value and energy dependence. An earlier attempt to calculate the cross section for this reaction analytically[29] gave poor agreement with experimental data, probably

[29] R. C. Koch and Anthony Turkevich, Bull. Am. Phys. Soc. Ser. II, 1, 94 (1956); R. C. Koch, Ph.D. thesis, University of Chicago, 1955 (unpublished).

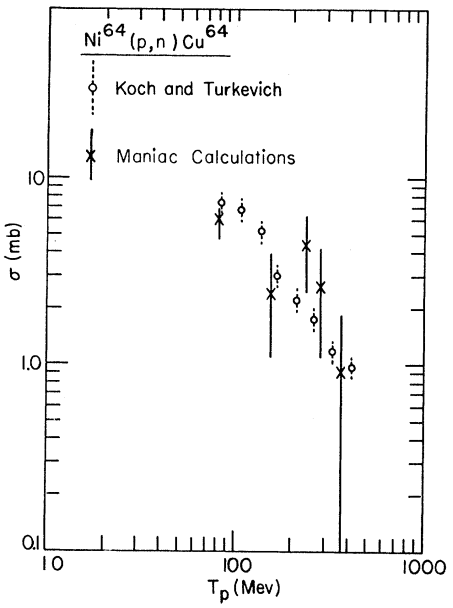

FIG. 20. $Ni^{64}(p,n)Cu^{64}$ reaction. Comparison between calculated and experimental results. The experimental data are those of Koch and Turkevich.[29]

because the angular dependence of the (p,n) scattering process was not properly taken into account.

Another simple reaction which can be compared reasonably directly with the results of the calculations is the (p,pn) process. There are three main mechanisms by which a (p,pn) product can be formed from a target nucleus. In one, the product results from a (P,PN) cascade, with the residual nucleus not having enough energy to evaporate further particles. In a second, there is a (P,P') cascade, with sufficient residual excitation to evaporate a neutron. This mechanism will be called the (P,P'_N) process. Finally, a mechanism consisting of a (P,N) cascade and subsequent proton evaporation—called the (P,N_P) process—can contribute.

The cross section for the $Cu^{65}(p,pn)Cu^{64}$ reaction has been calculated from the MANIAC results for copper and from evaporation theory. The evaporation widths of Blatt and Weisskopf[30] were modified to correct for the level densities in different types of product nuclei by taking the maximum particle energy to be 1 Mev greater than energetically possible in getting the evaporation widths for nuclei giving rise to odd-odd products, and 1 Mev lower than energetically possible when the product was an even-even nucleus. The results are presented in Fig. 21. This shows the calculated cross section in mb (ordinate) of the $Cu^{65}(p,pn)Cu^{64}$ process as a function of bombarding energy (abscissa) in the range 80 to 350 Mev. Also indicated are the contributions of the different mechanisms. These show the expected energy dependence. The experimental results shown are those of Yule and Turkevich.[31] It is seen that here, although the energy dependence is given correctly, the calculated results are too low by almost a factor of two. Approximate calculations indicate that this result applies to (p,pn) reactions in general—the calculated results starting from the MANIAC cascades are consistently low by similar factors. At the lower range of our energy scale this discrepancy might be attributed to contributions from pickup processes; an important addition to the cross section from this source at the highest energies seems improbable. Among the possible explanations is that a more realistic nuclear model with a diffuse edge extending to larger radii than used in this work might lead to enhanced contributions to specific reactions such as this (p,pn) process.

A final comparison with radiochemical results is an extremely crude calculation of the spallation yield mass curve for 340-Mev protons on copper. For this, the appropriate MANIAC results were combined with the following evaporation model: a unit mass change was assumed to take place for every 17 Mev of residual excitation. The results are shown in Fig. 22. This presents the cross section in mb as a function of the mass number of the product. The experimental results

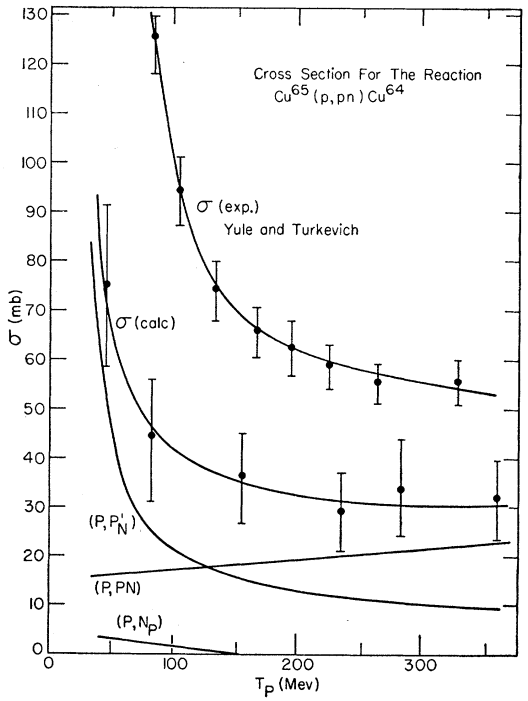

FIG. 21. $Cu^{65}(p,pn)Cu^{64}$ reaction. Comparison between calculated and experimental results. (The contribution of the three mechanisms to the calculated curve are shown.) The experimental data are those of Yule and Turkevich.[31]

[30] J. M. Blatt and V. F. Weisskopf, *Theoretical Nuclear Physics* (John Wiley and Sons, Inc., New York, 1952), p. 373.

[31] H. Yule and Anthony Turkevich (unpublished results), Enrico Fermi Institute for Nuclear Studies, University of Chicago, 1957; H. Yule, Ph.D. thesis, University of Chicago, 1957 (unpublished).

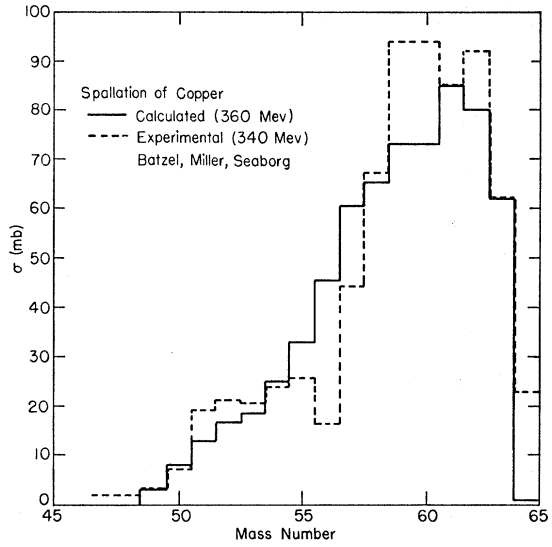

FIG. 22. Copper spallation by protons. Solid line: MANIAC calculation with 360-Mev protons and a crude evaporation model; dashed curve: Experimental data (including interpolated values) of Batzel, Miller, and Seaborg[32] with 340-Mev protons.

are those of Batzel, Miller, and Seaborg.[32] Since these workers used copper with a normal isotopic composition, the comparison at mass numbers above about 61 is not valid. It is seen that the main features of the experimental curve, namely, the high yields near the target mass, and the breadth of the distribution, are very well represented by the MANIAC calculations combined with the approximate evaporation treatment.

Moreover, our calculations show that the relative yields of various residual nuclei are rather insensitive to bombarding energy in the range between 200 and 350 Mev (Fig. 13). Likewise the excitation energy of these residual nuclei changes but little in this energy range (Fig. 15, Table IX, and Table X). Thus the calculation predicts that the main features of the spallation pattern of copper should not change significantly in the energy range 200 to 350 Mev. This is consistent with the impression of workers[33] in the field, although there appears to be no detailed experimental information on this point.

The three comparisons presented indicate that the model of high-energy nuclear reactions that forms the basis of the present calculation can account at least semiquantitatively for many features of spallation reactions. Consistent discrepancies between specific predictions of the calculation and experimental observations may be significant in indicating additional contributing mechanisms or in pointing the way toward refinements that should be introduced into the nuclear model used.

ACKNOWLEDGMENTS

The authors gratefully acknowledge the contribution of many of their colleagues during the course of this work. In particular the cooperation of J. Richardson and W. Orvedahl of the MANIAC engineering staff was indispensable. Dr. Jerome Friedman of the Enrico Fermi Institute for Nuclear Studies kindly had special photographic plates scanned for comparison with these calculations. The authors are indebted to Dr. W. C. Davidon for discussions related to the collision mechanics and to Dr. N. Sugarman and Dr. B. Pate for detailed criticisms of this report.

[32] Batzel, Miller, and Seaborg, Phys. Rev. **84**, 671 (1951).

[33] See, e.g., L. Marquez, Phys. Rev. **88**, 225 (1952).